Author for correspondence:
E. M. Campbell
e-mail: mcamp@lle.rochester.edu

Direct-drive laser fusion: status, plans and future

E. M. Campbell[1], T. C. Sangster[1], V. N. Goncharov[1], J. D. Zuegel[1], S. F. B. Morse[1], C. Sorce[1], G. W. Collins[1], M. S. Wei[1], R. Betti[1], S. P. Regan[1], D. H. Froula[1], C. Dorrer[1], D. R. Harding[1], V. Gopalaswamy[1], J. P. Knauer[1], R. Shah[1], O. M. Mannion[1], J. A. Marozas[1], P. B. Radha[1], M. J. Rosenberg[1], T. J. B. Collins[1], A. R. Christopherson[1], A. A. Solodov[1], D. Cao[1], J. P. Palastro[1], R. K. Follett[1] and M. Farrell[2]

[1]Laboratory for Laser Energetics, University of Rochester, 250 East River Road, Rochester, NY 14623-1299, USA
[2]General Atomics, 3550 General Atomics Court, San Diego, CA, 92121-1122, USA

(iD) EMC, 0000-0002-1220-6538

Laser-direct drive (LDD), along with laser indirect (X-ray) drive (LID) and magnetic drive with pulsed power, is one of the three viable inertial confinement fusion approaches to achieving fusion ignition and gain in the laboratory. The LDD programme is primarily being executed at both the Omega Laser Facility at the Laboratory for Laser Energetics and at the National Ignition Facility (NIF) at Lawrence Livermore National Laboratory. LDD research at Omega includes cryogenic implosions, fundamental physics including material properties, hydrodynamics and laser–plasma interaction physics. LDD research on the NIF is focused on energy coupling and laser–plasma interactions physics at ignition-scale plasmas. Limited implosions on the NIF in the 'polar-drive' configuration, where the irradiation geometry is configured for LID, are also a feature of LDD research. The ability to conduct research over a large range of energy, power and scale size using both Omega and the NIF is a major positive aspect of LDD research that reduces the risk in scaling from OMEGA to megajoule-class lasers. The paper will summarize

the present status of LDD research and plans for the future with the goal of ultimately achieving a burning plasma in the laboratory.

This article is part of a discussion meeting issue 'Prospects for high gain inertial fusion energy (part 2)'.

1. Introduction

In inertial confinement fusion (ICF), encapsulated fusion fuel is compressed and heated to extreme density, temperature and pressure so that the fusion reaction rate is rapid enough that significant energy release can take place before the fuel disassembles [1,2]. Depending on the details of the implosion, such as fuel mass, implosion geometry, and whether magnetic fields are employed, required imploded fuel pressures can range from tens to hundreds of gigabars. In the majority of current fusion research, the fuel is an equal molar mixture of the heavy isotopes of hydrogen (deuterium and tritium (DT)). In DT fusion, a total of 17.6 MeV of energy is released per reaction and carried off by a 14.1-MeV neutron and a 3.5-MeV alpha particle. The specific energy release from DT is approximately $4 \times 10^{11}\,\mathrm{J\,g^{-1}}$ [1,2]. The energetic uncharged neutron readily escapes the plasma (the range (areal density) in terms of parameters used in ICF as described below is approximately $10\,\mathrm{g\,cm^{-2}}$). By contrast, if the plasma is sufficiently dense, the alpha particles can be stopped and deposit their energy and rapidly heat the fuel. When this occurs, the fusion reaction rate rapidly increases (the reaction rate scales as the square of ion temperature, (T_i), for the range of ion temperatures of interest) and the energetics of the plasma becomes dominated by alpha self-heating [2]. For this to occur, in unmagnetized plasmas, the product of the areal density (ρR) and ion temperature (T_i) of the fuel, $\rho R T_i$, must exceed $(0.3\,\mathrm{g\,cm^{-2}}) \times (5\,\mathrm{keV})$ [2,3]. This generalized Lawson criteria (GLC) in ICF is equivalent to the $n\tau T_i$ of magnetic fusion, where τ is the energy confinement time and n is the particle density.

The GLC can also be written as $P\tau$, where P is the plasma pressure and τ is the plasma energy confinement time [3]. For alpha heating to dominate the plasma energetics as described above, $P\tau$ must exceed 10 atm-s with ion temperatures in excess of 5 KeV [$(P\tau)_{\mathrm{ign}}$ is defined at this value and is approximately 30 atm-sec at 5 KeV]. The $P\tau$ value is that achieved from the hydrodynamic work on the fuel by the implosion and is calculated in the absence of alpha heating. For ICF, the confinement time will be proportional to the imploded fuel radius (τ is effectively the time for a sound wave to transit the compressed fuel) and is in the range of $10^{-10}\,\mathrm{s}$ for unmagnetized plasmas, leading to fuel pressures in excess of 100 billion atmospheres.

Drivers such as lasers and pulsed-power systems that compress energy in space and time are required to produce such extreme conditions in the laboratory [4–6]. For laser-driven ICF, the concentrated energy flux generates pressure, P_{abl}, on the exterior of the target that implodes the fuel to the conditions required for fusion [3]. In laser-direct drive (LDD), the pressure is produced by the rapid ablation of the outer target surface by a high-intensity laser pulse. Peak laser intensity is typically in the range of $8\text{–}10 \times 10^{14}\,\mathrm{W\,cm^{-2}}$. In laser indirect drive (LID), the laser energy is first converted into X-rays in a high-Z enclosure (hohlraum) with an effective radiation temperature of approximately 300 eV. The X-ray flux then ablates the outer surface of the capsule. Figure 1 shows examples of ICF capsules for both LID and LDD that are designed for approximately 2-MJ, 350-nm lasers such as the National Ignition Facility (NIF) [5,6]. To maximize the implosion efficiency for both approaches, the ablators are low-Z materials such as plastic and carbon. In LDD [7,8], the initial CH ablator is thin so that the underdense corona consists of moderate charge-state (Z) ions to increase the inverse bremsstrahlung absorption (which scales as ion charge Z). To maximize the ablation pressure that scales as $(I_{\mathrm{abs}})^{2/3}(A/Z)^{1/3}$ (I_{abs} is the absorbed intensity and A is the atomic number of the ion) and efficiency of the implosion, most of the ablated mass is DT for LDD [8]. For all of these schemes, the ablation pressure given by the product of the mass ablation rate ($\mathrm{g\,cm^{-2}\,s}$) and the ablated material exhaust velocity is in the range of 100–150 million atmospheres. The implosion effectively serves as a 'pressure amplifier' to produce the extreme
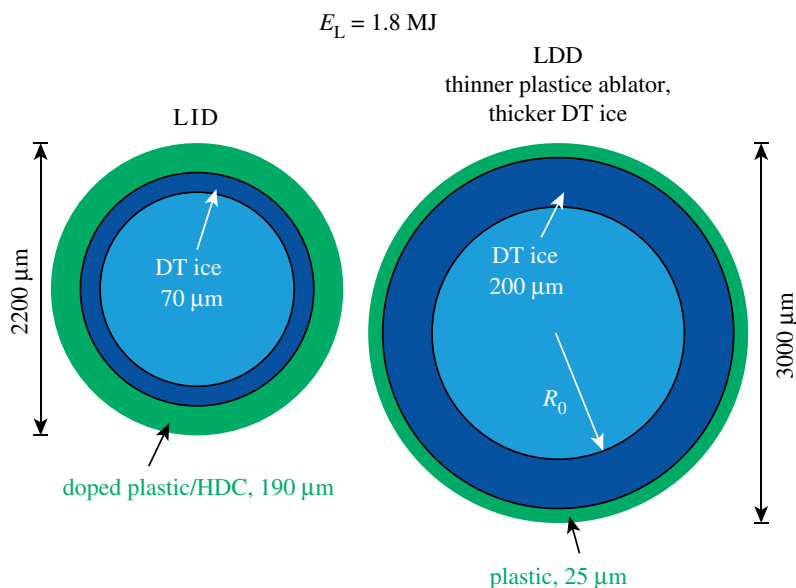
3

royalsocietypublishing.org/journal/rsta   *Phil. Trans. R. Soc. A* **379**: 20200001

$E_L = 1.8$ MJ

Figure 1. ICF cryogenic capsules for both LID and LDD designed for incident laser energies of 1.8 MJ. The more-massive LDD capsule is due to the larger energy coupled to the capsule. (Online version in colour.)

fuel conditions needed for fusion. In both laser approaches, these pressures produce implosion velocities, v_{imp}, in excess of 3.5×10^7 cm s^{-1} (greater than 10^{-3} of light speed). It is important to recognize that the ablation process is relatively inefficient with the kinetic energy of the imploding fuel being less than 20% (typically less than 10%) of the energy absorbed by the ablator [2,3].

Recognizing the overall inefficiency by which the energy from ICF laser drivers is coupled to the fusion fuel, in order to maximize the mass of DT that can be imploded and to minimize the size (and cost) of the laser, the implosion dynamics must be chosen to both ignite the fuel and, as described below, to compress sufficient mass so that significant energy release is possible [2]. The radial profiles of imploded fuel density and temperature to achieve significant energy release are shown in figure 2*b*. For a given target design, this near-isobaric imploded fuel assembly is achieved through temporal shaping of the laser pulse as shown in figure 2*a*. As described above, significant alpha-particle heating occurs in the central region when the GLC is met. This 'hot spot' is surrounded by cold nearly Fermi-degenerate fuel, where the pressure and density are related by $P_{Fermi} \sim \rho^{5/3}$. For the fuel to be degenerate, the quantity, $T(eV)^2 / \rho(g\,cm^{-3})^{2/3}$ must be of approximately 1 [2]. The ratio of the pressure in the cold fuel to the Fermi pressure, the adiabat α, is an important quantity describing the implosion dynamics and the amount of entropy added in the implosion process. High-performing implosions are designed with low adiabats since the lower the adiabat the higher the compressed fuel areal density and as shown below the fuel burnup [3]. The surrounding cold fuel confines (tamps) the igniting central hot spot and provides the majority of fusion fuel that enables high yield and gain [3].

If alpha heating in the central hot spot is sufficiently robust, a thermonuclear burn wave propagates into the cold fuel, producing large fusion yields. It can be readily shown that the fraction of the fuel in unmagnetized ICF targets that undergoes fusion (the burnup fraction, φ) depends on the total fuel areal density (which is dominated by the surrounding cold DT shell) and ion temperature:

$$\varphi = \frac{\rho R}{[\rho R + f(T_i)]} \tag{1.1}$$

where $f(T_i)$ which has units of g cm^{-2}, is approximately 6 for ion temperatures of interest ($f(T_i)$ relates the ratio of the DT fusion cross section to ion sound speed and is nearly constant for
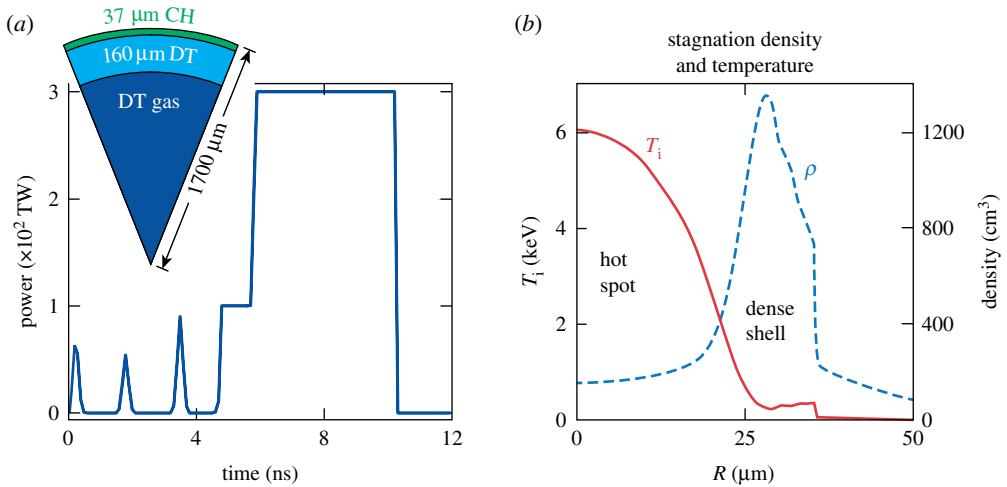
Figure 2. (*a*) Target and laser temporal profile that produces fuels conditions shown in (*b*) at stagnation; (*b*) radial profiles of ion temperature and density of the imploded DT fuel at stagnation. (Online version in colour.)

the range of ion temperatures expected in igniting ICF capsules) [2]. The total fusion energy produced in the implosion from a target of a given mass, m_{DT}, would simply be given by $\varphi \, m_{DT}$ (4×10^8) Joules with m_{DT} in mg. Given optimistic but credible driver energies, fuel masses and implosion physics, ρR values of 3 should ultimately be possible, resulting in a burnup fraction of 1/3. This would be a long-term credible goal for the ICF Programme. To release 100 MJ of energy if 1/3 of the DT underwent fusion would require approximately 0.75 mg of DT to be heated and compressed.

As mentioned above, the specific energy to compress the fuel is minimized when little entropy is added during the implosion and the fuel is nearly Fermi degenerate. This specific energy required to compress Fermi-degenerate DT is approximately given by ϵ_{Fermi} (J g^{-1}) $\sim 3 \times 10^5 \rho^{2/3}$ (g cm^{-3}). By contrast, the specific energy to heat DT, ϵ_{DT}, described by an ideal gas equation of state is ϵ_{DT} (J g^{-1}) $\sim 1.15 \times 10^8 \, T$ (keV) assuming equal electron and ion temperatures, T. This simple energetics argument defines the implosion strategy commonly used in ICF target designs. The target and temporal profile of the laser pulse as shown in figure 2*a* are designed so that in the final imploded configuration as shown in figure 2*b*, a small fraction of the fuel mass is compressed and heated to satisfy the GLC and the majority of the fuel is maintained as close as possible to Fermi degeneracy. Given the ratio of the specific energies, the 'energy partition' between the igniting hot spot and cold fuel is approximately equal.

An important metric to measure the progress in ICF research is given by χ, the ratio of the achieved $P\tau$ value to that needed for ignition [3,9]. As mentioned above, $P\tau$ is the value achieved by the hydrodynamic work done in the implosion. It can be shown that in the absence of alpha heating, this normalized general Lawson criteria can be expressed as

$$\frac{P\tau}{(P\tau)_{ign}} = \chi = \rho R^{0.6} \left[\frac{(\text{yield} \times 10^{-16})}{M_{DT}} \right]^{0.34}, \tag{1.2}$$

where ρR is in g cm^{-2} and unablated DT mass is in mg. Both the ρR and yield are experimentally measured and the unablated fuel mass is taken from simulations. When alpha deposition is sufficient to increase the fusion yield by approximately 3–4 over that which would occur from the hydrodynamic work on the fuel, a burning-plasma regime is reached. Alpha amplification refers to the ratio of the total fusion yield to that which is due to the hydrodynamic work alone. This occurs when χ is slightly greater than 1. Ignition occurs when a robust burning hot spot is formed, enabling a thermonuclear burn wave to propagate into the cold fuel. Ignition occurs when alpha amplification is greater than 15–25 [10].
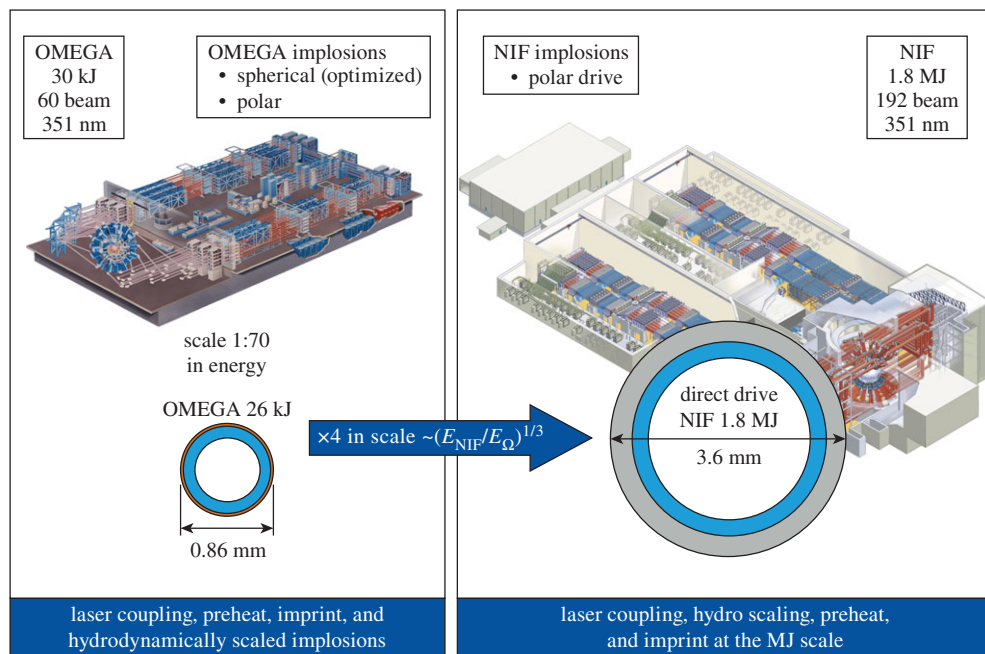
Figure 3. LDD research is conducted on both the 30-kJ, 30-TW OMEGA and 1.8-MJ, 500-TW NIF facilities. OMEGA is presently capable of both spherical and polar illumination but with only 2/3 of the laser energy. NIF illumination is optimized for cylindrical hohlraums and so is only presently capable of polar illumination for implosion experiments. (Online version in colour.)

In the following sections, progress in the LDD programme based on research at both the Omega Laser Facility and the NIF will be presented. The facilities and research topics are shown in figure 3.

The goal of the OMEGA research is to achieve the highest χ possible with the present facility and to understand degradation mechanisms that limit the implosion performance. This will be done both with spherical illumination for which OMEGA is optimized and then in the polar geometry that exploits the existing illumination geometry of the NIF [11]. OMEGA energy and power (30 kJ and 30 TW) are insufficient to achieve ignition conditions in the imploded fuel so both simulations and modelling are employed to scale OMEGA results to NIF energies (2.15 MJ and 500 TW). The LDD research on the NIF is focused on laser–target coupling and laser–plasma interaction (LPI) physics in ignition-scale plasmas. Implosions with limited convergence (less than 10), given the present capabilities of the NIF, are also a component of the research. The ability to conduct research over a large range of energy, power and scale size, using both Omega and the NIF, and the modelling and simulation tools developed at the Laboratory for Laser Energetics (LLE) are major positive aspects of LDD research that reduce the risk in scaling from OMEGA to megajoule-class lasers. The goal over the next decade is to develop and demonstrate a convincing physics case for modifying the NIF to enable burning-plasma experiments to be conducted, producing greater than MJ fusion yields from a direct-drive target illuminated in polar geometry [11]. An additional longer-term goal is to develop a quantitative understanding of LPI physics that limit the parameter space for all laser-driven ICF approaches and to develop and demonstrate advanced laser technology that can expand the parameter space and potentially lead to multi-megajoule yields and high fusion energy gain at MJ-scale laser energies.

The paper is organized as follows: §2 presents an overview of the physics and challenges of LDD; §3 describes the present status of OMEGA implosion experiments, the concept of hydro scaling and extrapolations to NIF energies and powers; §4 presents the LDD research on the NIF; §5 summarizes LPI research and plans including the development of a 'fourth-generation'
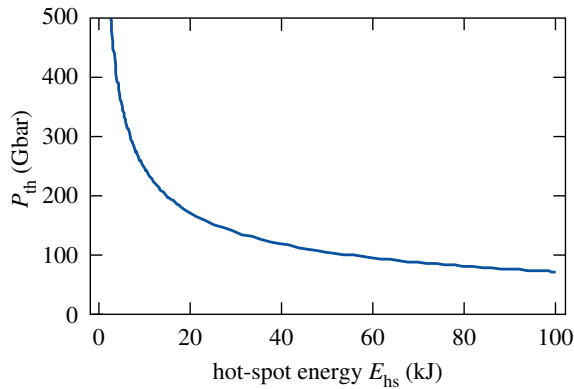
Figure 4. The hot-spot threshold pressure for ignition is reduced when more energy is coupled into the hot spot. The hot-spot energy coupled into an LDD capsule at NIF-scale energies would be in the range of 150 Gbar. (Online version in colour.)

laser-a broadband (bandwidth greater than 10 THz), 350-nm laser and; §6 summarizes the main conclusions of the paper.

2. Laser-direct-drive physics

The main advantage of LDD is the direct coupling of the laser energy to the target, enabling more mass to be imploded to fusion conditions [3,7,8]. The importance of this can be readily seen from the GLC for the hot spot. Relaying the threshold hot-spot areal density and temperature $(\rho RT)_{hs}$ to pressure and energy, it is straightforward to show that the hot-spot pressure (P_{hs}) must exceed the threshold pressure, P_{th},

$$P_{hs} > P_{th} = 250 \, \text{Gbar} \left(\frac{E_{hs}}{10 \, \text{kJ}} \right)^{-1/2}, \tag{2.1}$$

where E_{hs} is the energy in the hot spot. By coupling more energy into the hot spot, the required pressure, and therefore fuel convergence, for ignition is reduced (the hot-spot radius, R_{hs} scales as $(E_{hs})^{1/2}$). The large fuel mass (greater than 100 µg) that could be imploded in LDD with MJ-class laser drivers results in hot-spot ignition threshold pressures in the range of 150 billion atmospheres and capsule convergence (defined as the ratio of the initial outer shell radius to the imploded hot-spot radius) of approximately 20–25 for targets with multi-megajoule fusion output [7,8]. This simple relation is illustrated in figure 4 and shows the advantage of imploding more fuel mass made possible by coupling more energy. By imploding more mass for the same burnup fraction, higher yields and gain can be obtained for LDD even at a relatively high cold fuel adiabat. It is important to recognize that inferred hot-spot pressures well in excess of that needed for LDD at the MJ scale have been inferred in the laboratory. Pressures exceeding 300 Gbar have been measured, albeit in X-ray-driven implosions on the NIF [3].

In LDD, the overall efficiency by which the laser energy is delivered to the fuel is a product of three terms: absorption efficiency, rocket efficiency and the efficiency at which the kinetic energy of the imploding target is converted into internal energy of the fuel at stagnation [2,7,8]. Figure 2a above shows the nominal LDD target and laser pulse shape designed to achieve ignition and modest gain (5) at an incident 350-nm energy of 1.8 MJ and the sequence of physics that occurs in a laser-direct-drive implosion is shown in figure 5.

In the first stage of the implosion (figure 5a), the laser irradiates the ablator (plastic Be, Carbon) and generates an initial plasma most likely created by nonlinear processes such as multiphoton ionization. This early pulse launches a shock into the target and its timing relative to the main pulse along with the target ablator and DT ice thickness establishes the initial adiabat of the imploding shell. Given that in this early phase the plasma corona surrounding the target is small
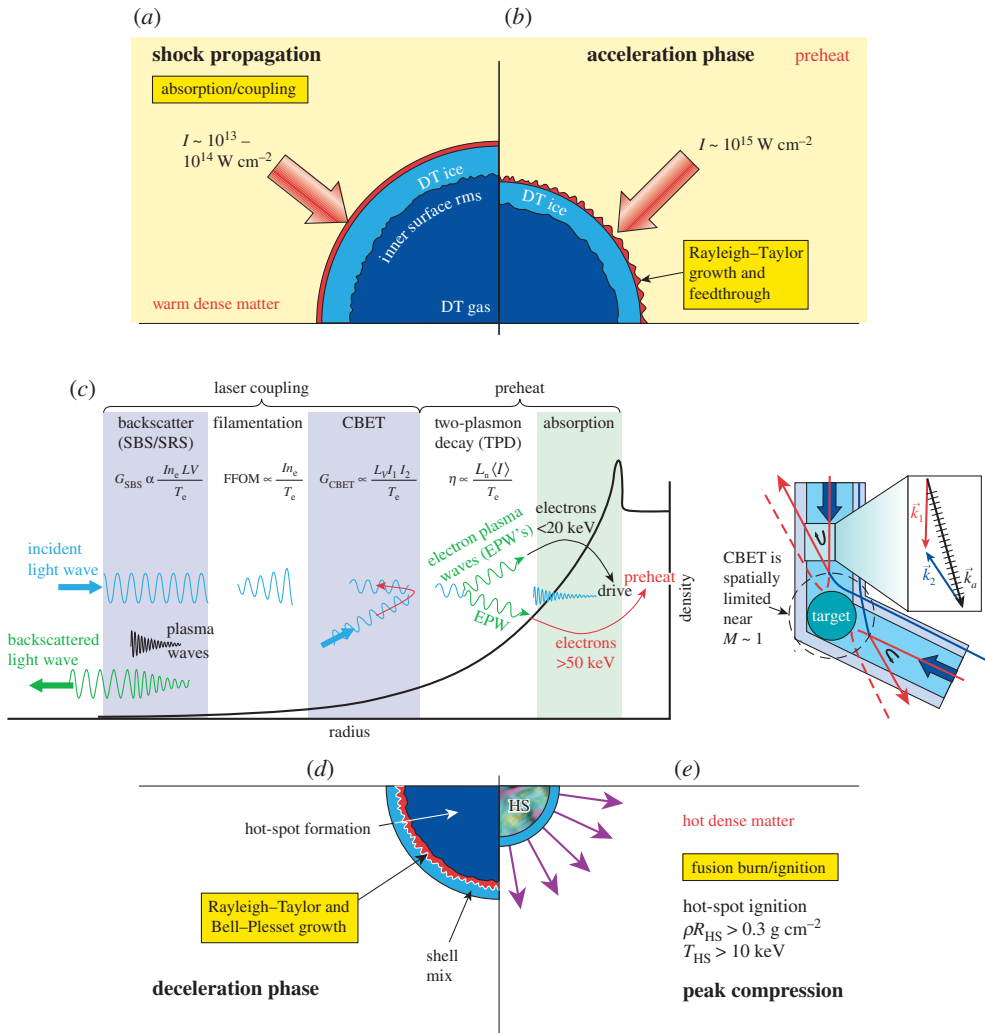
Figure 5. The four phases of an LDD implosion and the laser–plasma instabilities that can take place: (*a*) establishing the adiabat and seeds for hydrodynamic instabilities; (*b*) acceleration phase and laser peak intensity; (*c*) laser-driven instabilities that can occur during the acceleration phase; (*d*) deceleration phase and (*e*) stagnation and fusion production. (Online version in colour.)

and there is little distance between the absorption region and the ablation surface, any non-uniformities in the laser will result in mass perturbations that can seed hydrodynamic instabilities (discussed below). Significant advances in ICF lasers have been made in past decades to reduce the laser non-uniformities, including distributed phase plates (DPP's) that reduce the spatial coherence of the laser and match the far-field laser profile to the target dimension [12]. As a result, DPP's produce well-defined 'noise sources' that are at high spatial frequencies ($k \sim 2\pi /f^{\#}\lambda_{\text{laser}}$, where $f^{\#}$ and λ are the f number of the focusing optic and laser wavelength, respectively) due to the speckle caused by the coherence of the laser. Techniques that 'move the speckles' at a rate determined by the laser bandwidth such as smoothing by spectral dispersion (SSD) and induced spatial incoherence have also been developed and implemented in modern ICF drivers [13,14]. In addition to laser-induced noise sources, any defects in target fabrication or surface particulates that accumulate during the fueling and fielding of the target can also serve as seeds for hydrodynamic instabilities that occur during the implosion. Since the laser directly illuminates

Table 1. Plasma corona conditions for the NIF and OMEGA experiments.

	NIF ignition scale	ongoing NIF planar experiments	ongoing NIF implosions	OMEGA experiments
density scale length at L_n (µm)	600	400–700	360	150
electron temperature, T_e (keV)	3.5–5	3–5	3.2	2.8
overlapped peak beam intensity, I_L (W cm^{-2})	$(6-8) \times 10^{14}$	$(6-15) \times 10^{14}$	$(5-8) \times 10^{14}$	$(5-8) \times 10^{14}$

the target, low-mode drive non-uniformity (where mode number, $\ell = 2\pi R_{cap}/\lambda_{spatial}$ where R_{cap} is the capsule radius and $\lambda_{spatial}$ the mode wavelength) caused by laser power imbalance, variations in absorption due to LPI physics in the plasma corona, target placement, beam mis-pointing, or the beam geometry with a finite number of beams is also a concern for LDD [7,8]. OMEGA has 60 beams arranged in a truncated icosahedron pattern (similar to a soccer ball) that leaves a low-level residual mode 10 even when all other sources are zero [15]. These low modes generally grow secularly in time and can be enhanced by the Rayleigh–Taylor instability and Bell–Plesset growth during the implosion process. Such low-mode non-uniformities can result in incomplete conversion of the imploding shell kinetic energy into pressure at stagnation and degrade the overall fusion performance [3].

In the next phase of the implosion (figure 5b), the laser intensity rises to its peak value and the target accelerates to its peak velocity, which is typically in excess of 3.5×10^7 cm s^{-1} [3,7,8]. The peak incident laser intensity summed over multiple beams is approximately 10^{15} W cm^{-2}. This is the so-called 'hard sphere' intensity that is calculated at the initial target surface. A large and hot corona surrounding the target will be established during this phase. Table 1 shows nominal values of the electron density and temperature for different classes of targets shot on OMEGA and the NIF. For capsules, the spherical divergence of the plasma flow will result in plasma scale lengths of a fraction (approx. 1/3) of the target radius.

The laser–target coupling takes place in this corona up to the critical electron density ($n_c \sim 10^{21}/\lambda^2$, where n_c is e/cm^3 and λ is in µm). Figure 5c schematically shows the processes that take place in the surrounding underdense plasma corona [16]. Ideally, the laser–plasma coupling will be dominated by inverse bremsstrahlung (collisional) absorption. In the absence of any LPI, absorption efficiencies greater than 90% would be expected. However, the multibeam irradiation of LDD enables processes such as cross-beam energy transfer (CBET) [17,18] that can significantly reduce the target absorption and increase low-mode drive uniformities even with 'perfect' power balance and target positioning. CBET is simply seeded Brillouin scattering (SBS) in which an incoming laser beam that is refracted in the underdense corona or reflected/scattered off the critical surface serves as a 'seed' for incoming light from another laser beam. In addition to CBET, another major concern are high-frequency instabilities such as the two-plasmon decay and stimulated Raman scattering (SRS) that produce energetic electrons with nominal temperatures of approximately 40–50 keV that can preheat and reduce the compressibility of the fuel. This energy deposition raises the entropy and increases the adiabat of the fuel. The generation and transport of these energetic electrons to the cold fuel are important research topics for LDD.

During this phase, the target accelerates to the maximum implosion velocity. It is also classically hydrodynamically Rayleigh–Taylor (RT) unstable since at the ablation surface, the lower-density ablation plasma, is accelerating the dense inner fuel [3,7,8]. As mentioned above the RT instability amplifies the initial noise sources arising from laser imprint, roughness on the target surface or imperfections (voids) in the shell, and any debris that the target collects during fueling.

Figure 5d schematically illustrates the deceleration phase of the implosion. As the target continues to implode, the inner fuel being essentially adiabatic, the pressure increases as $V^{-\gamma}$ [8]. When the pressure becomes sufficiently high, the shell begins to decelerate and the central hot-spot ignition region begins to form. Perturbations that have grown during the acceleration phase

feed through to the inner shell and serve as seeds again for RT unstable growth (the hot-spot density is lower than the dense shell) that can be modified by Bell–Plesset effects [7,8].

Achieving a robust hot spot is extremely challenging (figure 5*e*). Mix of the cold fuel into the hot spot resulting from the RT instability can quench the burn and the bubble and spike structure of the perturbed hot spot–cold fuel interface can increase electron conduction losses from the hot central plasma. If severe, the RT instability can break up the cold fuel shell. As discussed above, low-mode drive non-uniformities can also result in incomplete stagnation. When this occurs, not all of the implosion kinetic energy is converted into pressure and significant residual kinetic energy can result, effectively reducing the efficiency of the 'pressure amplification' of the implosion [19,20].

3. OMEGA implosion experiments and hydro scaling to MJ laser drivers

High-performance cryogenic implosion experiments scaled to the 30-kJ, 30-TW OMEGA laser are routinely conducted at LLE. The multi-year strategy of the OMEGA implosion campaign includes: finding the optimum implosion with spherical illumination; determining degradation mechanisms and developing mitigation strategies; extrapolating the spherical illumination implosion performance on OMEGA to NIF energies and powers (2 MJ and 500 TW) by hydro scaling; and determining the impact of present NIF-like polar illumination [21].

Despite the significant progress in modelling and analysing ICF implosions with multidimensional radiation-hydrodynamic (RH) codes over the past decades, it is still not possible to accurately predict the results of implosion experiments. The reason for the inability is the enormously complicated, interconnected, nonlinear physics occurring in three dimensions, of the four stages of a direct-drive implosion illustrated in figure 5. Another complexity that must be considered in developing an implosion strategy is the large parameter space that is available in experiments, including the details of the laser temporal pulse history and the dimensions and composition of the target. The relatively limited number of implosion experiments even at OMEGA that are possible in present ICF facilities limits the ability to explore the extensive target design parameter space for optimizing performance.

Given the above motivations, we have developed a strategy that exploits our understanding of the physics of ICF implosions and mines the database, flexibility and reproducibility of OMEGA. A data-driven predictive machine-learning approach has been developed to optimize the implosions exploiting the capabilities of the Omega Laser Facility [22]. The goal of this programme is to not only find the optimal implosion, but as mentioned above, understand degradation mechanisms and develop and demonstrate mitigation strategies.

The strategy consists of the following elements [22]. The 1-D code *LILAC,* in which the input parameters (target, laser pulse) are specified, is used to explore the implosion performance over a range of initial conditions that time and resources would not allow to be explored experimentally or with multidimensional RH codes. Observables (yield, areal density, etc.) are then calculated, which are a function of the input parameters alone since three-dimensional (3-D) effects and the resulting physics are not included. As described by Gopalaswamy [22], with a large number of simulations, a function relating the simulated observables, O^{sim} to the one-dimensional (1-D) input conditions can be constructed

$$O^{\text{sim}} = F_{\text{sim}}(I_{\text{1-D}}). \tag{3.1}$$

The observables measured (O^{exp}) in an actual experiment of course do not match the simulated ones because of 3-D effects (and perhaps gaps in physics understanding such as particle transport, magnetic fields, kinetic effects such as species separation to name but a few). The strategy that we have developed to optimize implosions is to construct a predictive model that describes experimental measurements as a function of the simulated 1-D observables and 3-D physics. As discussed in [22], the function F_{sim} can be inverted and the experimental observables can then be

described by

$$O^{\text{exp}} = F_{\text{exp}}[F_{\text{sim}}^{-1}(O^{\text{sim}}), F_{\text{3-D}}], \tag{3.2}$$

where F_{3-D} is a function that describes 3-D physics and is determined by both modelling and through well-controlled and diagnosed experiments. An example of 3-D physics that would not be included if only 1-D output would be used, would be mass perturbations seeded by laser imprint and subsequent RT growth, leading to mix or shell breakup. Given the repeatability of OMEGA, this is an example of a systematic 3-D effect. As shown in figure 6a, it is also something that can be systematically varied by modifying the beam smoothing system (2-D SSD) on OMEGA and seeing the effect on experimental observables such as yield and areal density, and then incorporating into the model (J. P. Knauer 2020, private communication). Random 3-D effects also occur in experiments, such as having the target placed off-center, resulting in low-mode drive asymmetries. As mentioned above, this asymmetry leads to incomplete stagnation, where a significant amount of the implosion energy resides in fuel kinetic energy rather than pressure. With multiple line-of-sight diagnostics that infer the residual kinetic energy in the fuel, it is possible to infer this 3-D effect, which can also then be incorporated into the model. The systematic experiments demonstrating the impact on yield from both gas and cryogenic targets from λ-mode 1 are shown in figure 6b,c [19]. The experimental parameter from which the residual kinetic energy is deduced is the ratio of the maximum to minimum inferred ion temperature, determined from multiple neutron time-of-flight detectors [19,20].

Figure 7 shows the results of this strategy, where the fusion yield from over 160 implosion experiments are compared with the model predictions. This statistical model incorporates not only 1-D physics, but includes the impact of 3-D effects as discussed above. These implosions include a wide range of '1-D' input parameters (laser pulse shape and target details (DT ice thickness), capsule radius and ablator thickness), and 3-D effects such as imprint (by varying the level of SSD smoothing) and low-mode drive uniformity (due to target placement and varying the ratio of the laser beam to target radius employing different phase plates). The impact of fuel age—the time between fueling and conducting the implosion—are also included. Experiments on OMEGA will continue to be added to the database and modelled over the next several years. Additional diagnostics focusing on 3-D effects will continue to add more observables and further refine the model [21].

The next step in the strategy is to project the OMEGA performance to NIF-scale energies and powers (2.1 MJ, 500 TW) [23]. The assumptions are as follows: the illumination geometry is similar to OMEGA; the target mass and volume scale with energy so that dimensions, laser pulse and time profile scale as $(E_{\text{NIF}}/E_{\text{OMEGA}})^{1/3}$, the energy coupled to the target is the same (J g^{-1} is invariant); the implosion velocity and adiabat are the same; the final hot-spot pressure and cold fuel density are the same (the pressure at the NIF scale is slightly higher due to smaller conduction losses given the smaller surface/volume ratio compared to OMEGA); and all target non-uniformities (DT and ablator roughness, fill tube to fuel the target or mounting stalk) scale with size. This last assumption should be conservative since DT ice and ablator roughness for OMEGA-scale targets are similar to that presently shot on the NIF and in ignition-scale LDD target fabrication research. Target mounting and fill tube dimensions will also be minimized and will not simply scale with $(E_{\text{NIF}}/E_{\text{OMEGA}})^{1/3}$.

This hydro scaling also assumes that the level and impact of LPI and the laser–target coupling are the same at the OMEGA and NIF scales. As discussed in §4, MJ-scale targets and plasmas will be 3–4× larger than those on OMEGA. The history of the ICF Programme has shown that to be a dangerous assumption and is a major motivation for conducting experiments on the approximate 2-MJ, 500-TW NIF. The NIF at present is also not optimally configured for LDD. The beam smoothing capability is far inferior to that on OMEGA, resulting in enhanced sources for hydro instabilities and the intensity on target has significant amplitude modulations that can drive LPI. Experiments have shown, that particularly near threshold, that instabilities are driven by the larger localized intensities rather than the spatially averaged value. As shown in figure 8a, the illumination geometry of the 192 NIF beams is also arranged for cylindrical
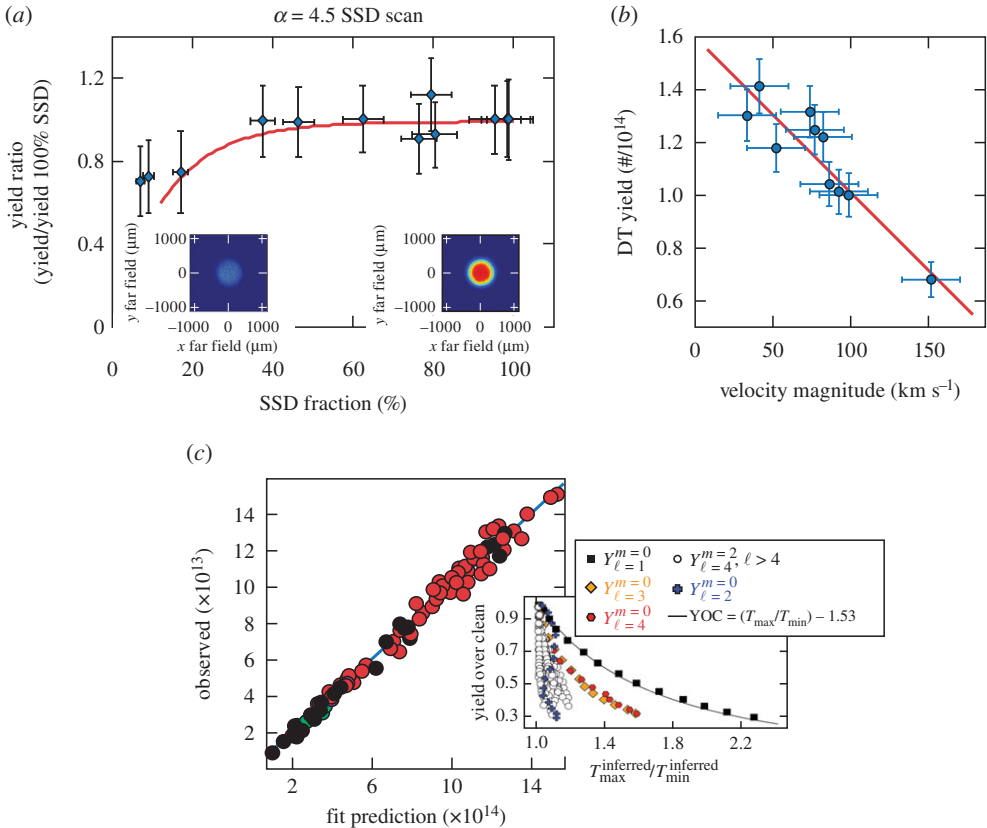
Figure 6. (*a*) Impact of laser imprint on implosion performance is systematically explored by varying levels of SSD beam smoothing (target plane time integrated beam profiles are also shown with SSD on and off (DPP alone)); (*b*) impact of low-mode drive non-uniformity and residual fuel kinetic energy on fusion performance with gas-filled targets; (*c*) experiment and modelling comparison of fusion performance when residual kinetic energy is inferred from the ration of the maximum to minimum ion temperature diagnosed by neutron time-of-flight detectors. The inset shows the expected yield reduction as a function of this ratio. (Online version in colour.)

or near-cylindrical hohlraums [5,6]. While the NIF target chamber has ports that would enable symmetric illumination, the nearer-term option for LDD is to develop polardirect drive (PDD) and to execute experiments on both OMEGA and the NIF with this illumination geometry [7,21] The beam pointing for polar drive is shown in figure 8*b* and the time integrated spatial energy profile is shown in figure 8*c*. The LDD programme will address the level of beam quality needed for NIF for both laser imprint and LPI mitigation. Beam smoothing similar to that on OMEGA (2D SSD, polarization smoothing) will be evaluated for the NIF over the next several years motivated by the ongoing research programme.

Despite these caveats and assumptions, hydro scaling is an important tool for projecting OMEGA performance to the energy and power levels of ignition-scale facilities. Figure 9*a* shows the scaling of χ which scales with laser energy as $\sim E_L^{1/3}$ (target absorption is assumed to be similar at both scales) and figure 9*b* shows the yield scaling with and without alpha heating. At NIF-scale energies (2 MJ), the alpha amplification is approximately 3, giving projected yields of approximately 600 kJ. The research on OMEGA over the next several years will be to exploit 3-D diagnostics and improved target fabrication to achieve scaled $\chi > 1$ and to understand and mitigate degradation mechanisms including performance penalties due to polar illumination [21].
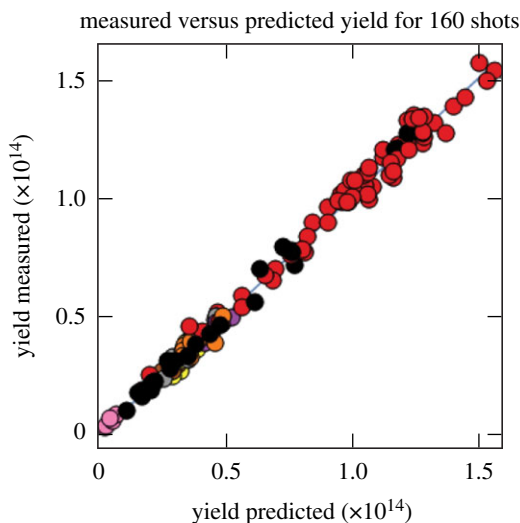
12

royalsocietypublishing.org/journal/rsta   *Phil. Trans. R. Soc. A* **379**: 20200011

Figure 7. Comparison of data-driven statistical model with actual experimental fusion yields. Over 160 experiments are well described by this predictive model with a wide range of parameters as described in the text. (Online version in colour.)
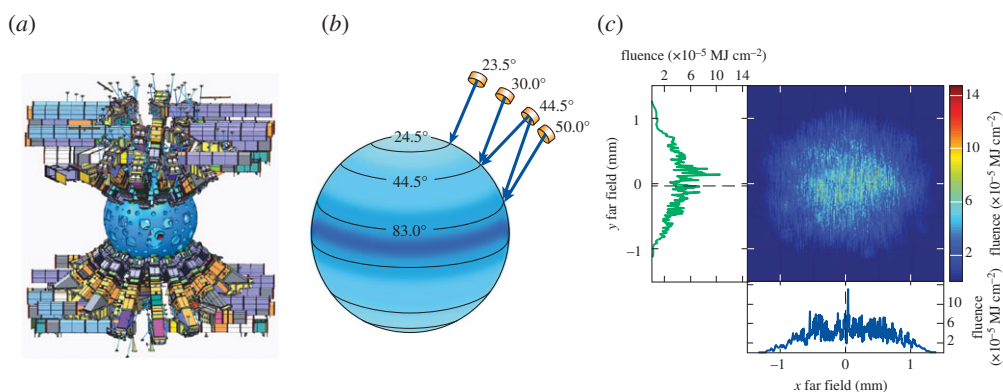

Figure 8. (*a*) The present illumination geometry for NIF is arranged for cylindrical or near-cylindrical hohlraums. LDD implosion experiments that use this geometry are referred to as PDD; (*b*) the beam pointing for NIF for PDD; (*c*) nominal equivalent-target-plane fluence for NIF beams for LDD research. The beams have significant spatial fluence modulations that influence LPI particularly near threshold intensities. (Online version in colour.)
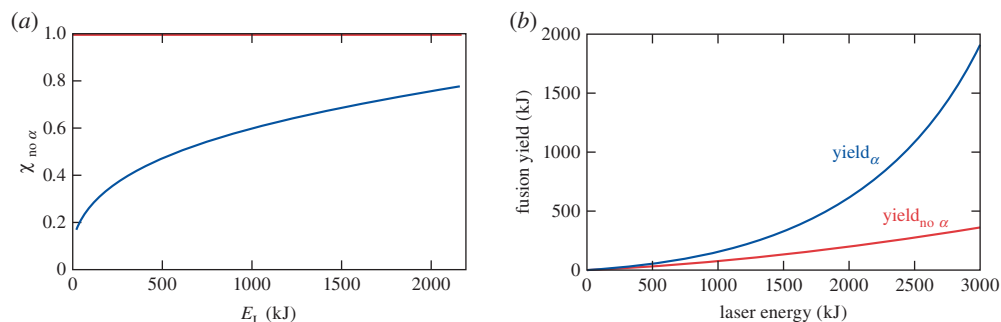
Figure 9. (*a*) Energy scaling of ignition metric χ based in series of highest performing OMEGA experiments to NIF energies; (*b*) fusion yield scaling with energy with and without alpha amplification. (Online version in colour.)

4. Direct-drive research on the NIF

As discussed above, a major advantage and key strategy of the LDD Programme is the ability to conduct research on both OMEGA and the NIF. Although at present not configured for LDD (illumination geometry, beam conditioning), experiments on the NIF explore LPI and target-coupling physics at ignition-scale plasmas. In addition to these physics objectives, limited performance implosions in the NIF polar-configuration illumination geometry are also studied to develop neutron sources and test/validate codes. As described in §3 on hydro scaling, scaling from OMEGA to the NIF involves a fourfold increase in target/plasma corona dimensions and a corresponding increase in laser energy and power by factors of 70 and 15, respectively. The same modelling and analysis tools are used to design and to develop an understanding of experiments conducted at both facilities. This capability did not exist in the physics programme leading to the NIF since only the 30–40 kJ, 10 beam NOVA [24] laser was available prior to the construction of the NIF.

Figure 8 above shows the present beam geometry for the NIF that was designed for irradiating cylindrical hohlraums for X-ray-driven implosions and the beam pointing and beam quality that is used for PDD implosions. A range of targets including planar foils, solid spheres and capsules are used in the LDD programme. Table 1 shows the laser and plasma conditions in the underdense corona for a variety of targets. These parameters are critical in determining the mix of laser–plasma coupling physics shown in figure 5c, that influence the design space available for LDD implosions. It is important to recognize as was mentioned above, that the poor quality of the NIF beams (shown in figure 8c) with DPP designed for indirect drive and minimal temporal beam smoothing will also increase the levels of LPI compared to that which would occur with the beam smoothing required for LDD. As a result, the NIF LPI studies will result in 'worst-case scenarios'. The goal of these experiments is to help define the laser–target parameter space available for LDD designs that include high-adiabat, low-convergence implosions to targets that ignite producing MJ and greater fusion yields [21].

With the above caveats, the majority of LDD experiments on the NIF to date have focused on laser–plasma coupling with a specific focus on instabilities such as the two-plasmon-decay instability ($2\omega_{pe}$) and SRS that produce energetic electrons that can preheat and reduce the compressibility of the imploding DT shell [25]. Another process of concern to all laser-driven approaches that is being addressed on the NIF is CBET [17,18]. CBET leads to energy exchange between beams seeded by stimulated Brillouin scattering (SBS). For LDD, CBET can lead to a reduction in target absorption and modifications in the absorbed intensity spatial profile that can lead to time-dependent drive asymmetries. For beams of identical frequency, CBET occurs at the Mach 1 region of the expanding plasma corona. If the beams are at different frequencies, then the resonance moves to lower gain regions in the corona reducing the impact of CBET. Unlike the 60-beam OMEGA laser at LLE, the NIF does have a limited ability to operate the individual beams at slightly different wavelengths. Present capability limits this wavelength detuning to ±2.3 Å [26]. Modelling of high-performing LDD targets at MJ laser energies indicates that a minimum detuning of ±6 Å is required [27]. Ongoing modelling and experiments at the TOP9 facility at LLE discussed below and the NIF will further refine and quantify the required detuning.

Figure 10 summarizes a key result from CBET experiments in the NIF exploiting the wavelength detuning capabilities [18]. The figure shows X-ray radiographs of 'polar-drive' imploding shells when the beams from the top and bottom hemispheres that irradiate the equatorial region of the target where CBET is most effective are detuned. The figure shows the design prediction from the *DRACO* code that includes CBET and nonlocal electron transport and the measurement of the equatorial mass accumulation near the equator due to increased absorption (CBET reduction) from the wavelength detuning of the equatorial beams by ±2.3 Å. Other observables such as scattered light and the shell trajectory in the equatorial region are also well matched by the simulations. Future experiments with more flexibility in the beam strategy for detuning are being planned and discussions to expand the wavelength separation are ongoing.
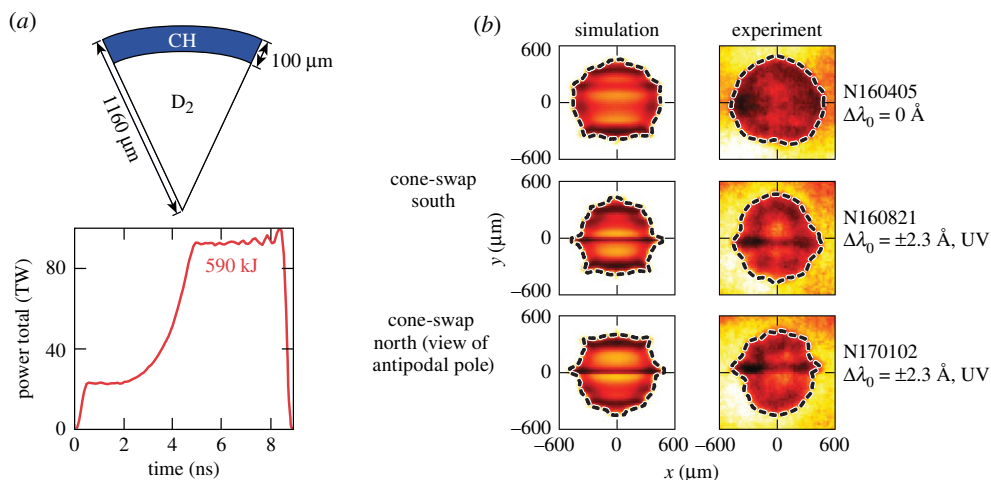
Figure 10. (*a*) Experimental set-up for CBET experiments on NIF (target and laser pulse); (*b*) radiographs and simulations of imploding targets with and without wavelength detuning showing effects of CBET reduction at the equator. The mass pileup on the equator shown in the radiographs is a result of more laser absorption at the equator. (Online version in colour.)
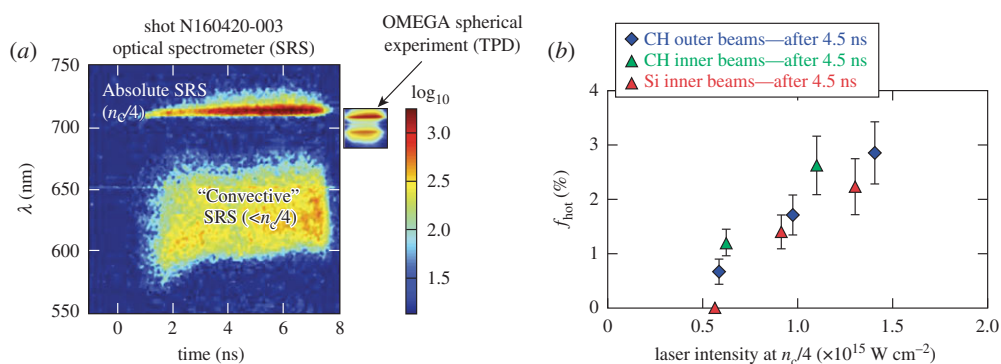

Figure 11. (*a*) Scattered-light spectrum from OMEGA and the NIF. The half-harmonic spectrum at OMEGA is characteristic of the two-plasmon-decay instability while the broad spectrum at 600–650 nm is characteristic of convective SRS at electron densities $<n_{\rm c}/4$ (*b*) Hot-electron levels inferred from hard X-ray measurements from planar targets where CBET is negligible. The data are taken with 4.5 nsec pulses and with CH targets (one with a thin Si overcoat). The inner and outer beams refer to the different NIF beam cones [25]. (Online version in colour.)

Figure 11 summarizes hot-electron experiments executed on the NIF that are discussed in detail in the references [25,28]. Not surprising, the scattered-light spectrum (figure 11a) from the large coronas from irradiated planar targets (table 1) where CBET is negligible, shows that SRS occurring in plasma densities less than $n_{\rm c}/4$ is the dominant source of the approximately 40–50 keV hot electrons [16,29]. In the smaller plasmas on OMEGA, the two-plasmon-decay instability is dominant [30,31]. Hot-electron levels deduced from hard X-ray emission (figure 11b) can be as large as several per cent of the laser energy if the laser intensity is greater than $5 \times 10^{14}\,{\rm W\,cm^{-2}}$ at $n_{\rm c}/4$ [25]. These results show the importance of conducting experiments at the MJ scale even with the poor-quality NIF beams.

The impact on implosion performance must include not only the production of the energetic electrons in the underdense corona but also their transport to the imploding DT shell as shown schematically in figure 12a. In order to determine the level of preheat in the DT shell, experiments have been designed and executed on both OMEGA and the NIF using CH targets with high-Z
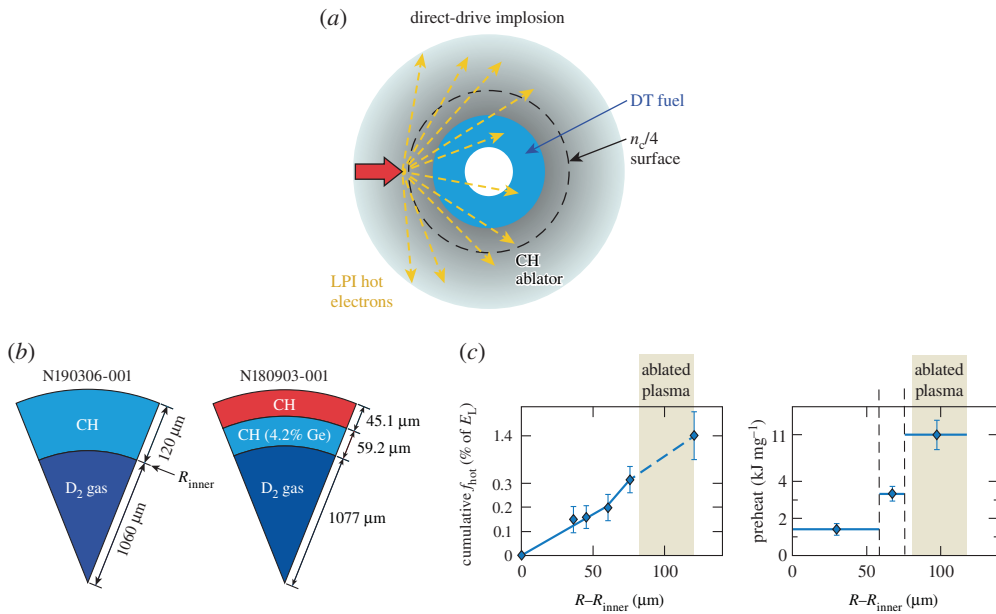
Figure 12. (*a*) Schematic showing that the preheat to the cold shell is a function of both the amount of hot electrons produced, the angular spread of the source, and the transport to the cold shell. (*b*) Targets with high-*Z* doping are located at different radial positions in the target and the energy deposited is inferred from the differential X-ray yield. (*c*) Radial distribution of preheat inferred by differential X-ray yield from radially located Ge-doped CH targets. (Online version in colour.)

layers located at different radial positions [32]. By measuring and comparing the X-ray fluence from these different targets, the radial distribution of the hot-electron deposited energy can be inferred as well as their effective angular spread from the region of the corona where they are generated. Similar to that found in earlier OMEGA experiments, recent NIF experiments have inferred that the energetic electrons are emitted with a large divergence, nearly uniformly into the forward 2π [31]. The preheat levels are therefore reduced when the distance between the cold shell and the underdense ($n_e < n_c/4$) corona, where SRS is occurring increases and the subtended solid angle of the inner DT shell is reduced. Figure 12*b,c* shows a schematic of the experiment and the initial results of NIF experiments where the peak laser intensity, similar to that employed in the OMEGA cryogenic experiments is approximately $8 \times 10^{14}\,\mathrm{W\,cm^{-2}}$. The levels of preheat in the inner region of the shell is approximately 1 to $2\,\mathrm{J\,\mu g^{-1}}$ [21,32] (A. Solodov 2020, private communication). While this is comparable to that seen on OMEGA, it is important to note that the electron transport from the corona involves CH, whereas in a well-designed cryogenic implosion the majority of the corona is lower atomic number, DT. Cryogenic direct-drive targets are not yet possible on the NIF. Over the next several years, these experiments will expand to include a range of intensities, corona conditions and varying radial distances of the high-Z diagnostic layer from where the hot electrons are produced [21].

The present capabilities on the NIF as discussed above significantly limit the ability to do high-performance, direct-drive implosions. In addition to the laser issues, there is presently no capability to field cryogenic targets on the facility. The original vision/plan for the NIF was to explore a variety of target concepts including direct drive. While the NIF has target chamber ports for spherical illumination, the near-term focus will continue to be PDD.

Even with these limitations, it is still valuable to design and conduct implosion experiments. While limited to low-convergence (less than 10), high-adiabat implosions with gas-filled targets as mentioned above, these experiments enable integral tests of the RH simulation codes including laser–target coupling, which includes CBET and nonlocal electron transport, implosion
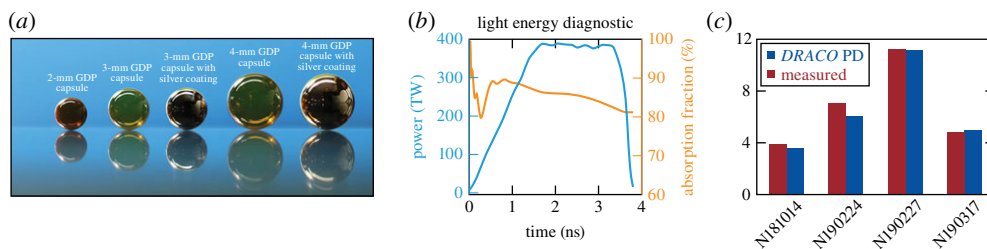
Figure 13. (*a*) Three to 4-mm-diam DT-filled capsules for PDD experiments. (*b*) NIF laser pulse and calculated absorption fraction as a function of time. (*c*) Measured and 2-D simulations (including CBET and nonlocal electron transport) of fusion yield. (Online version in colour.)

hydrodynamics, stagnation and fusion production. Figure 13 summarizes recent results on these PDD implosions [33]. The plastic capsules filled with approximately 8 atm of equimolar DT shown in figure 13*a* are nominally 3–4 × larger than those shot on OMEGA as would be expected from hydro scaling. A representative pulse shape and calculated absorption time history is shown in figure 13*b* with total on target energy of approximately 1 MJ with peak power of 400 TW. Both of these values are well below NIF performance limitations. Figure 13*c* shows the yield calculated by the 2-D code *DRACO* compared with the measured yields. There is good agreement between modelling and simulations with a highest measured yield of 1.1×10^{16} neutrons (approx. 31 kJ of fusion energy produced). Other observables are in good agreement such as the time of neutron emission (bang time), which is related to target absorption (calculated to be greater than 80%). Given the highly 3-D nature of the implosion a quantitative comparison with all observables (time history of the neutron emission, ion temperature) with a 2-D code is not to be expected. Nonetheless, the results to date are encouraging and serve as a motivation to improve NIF capabilities such as increased wavelength separation and customized DPP that are optimized for polar-direct-drive implosions with 3- to 4-mm-diam targets. Experiments over the next several years will explore optimized laser pulse shapes and improved beam wavelength mapping with a goal of achieving fusion yields of 100 kJ (neutron yield of 3.54×10^{16}) [21].

5. Laser–plasma interaction research

Understanding the physics of laser-driven parametric instabilities (LPI) and the limitations they place on the laser–target parameter space available for high-performance implosions has been an active topic of ICF research over five decades [16]. The coupling physics have always impacted the choices of laser technology for ICF. ICF research began with high-power Nd:glass and CO_2 lasers with output wavelength of 1.05 μm and 10.6 μm, respectively [2]. Poor coupling observed in numerous experiments worldwide led to the elimination of CO_2 lasers and frequency up-conversion to the third harmonic (0.35 μm) has maintained Nd:glass lasers (NIF, OMEGA, LMJ, SGIII) as the primary laser technology for ICF research [5,6,15,24,34,35]. Short wavelength (approx. 250 nm) LDD planar experiments are also conducted on several kJ KrF Nike laser at the Naval Research Laboratory (NRL) [36].

Given the importance to the field and complexity of the physics, LLE has developed a broad, multi-year strategy for LPI research [21]. The physics that occur in the underdense corona, schematically shown in figure 5*c*, is extremely complex. The physics depends on the corona density, temperature and velocity profiles, the energy distribution function of the electrons and ions (which are generally not Maxwellian), and the details of the laser irradiation on target (intensity, wavelength, polarization, beam quality, beam overlap). In addition, there are multiple processes ongoing and competing with one another and they occur on time and space scales measured in sub-picosecond and micrometres, respectively. In order to develop a quantitative and scalable (from OMEGA to MJ energy lasers) understanding of LPI, the research programme
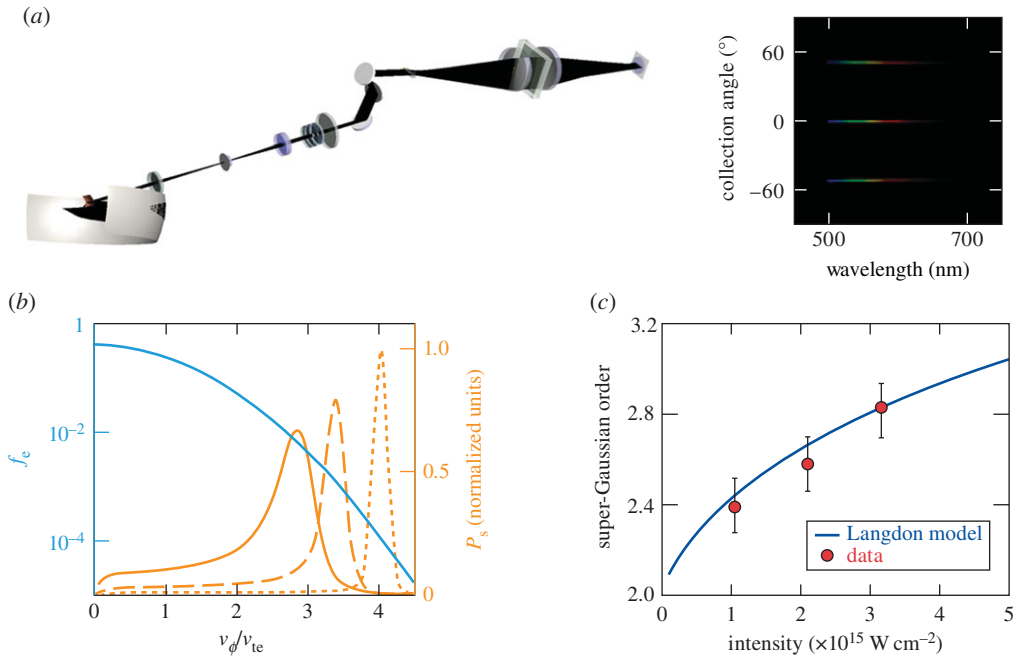
Figure 14. (*a*) Schematic and scattered Thomson-scattered light measured over 120°; (*b*) schematic showing that scattered light from different angles selects different regions of the EDF; (*c*) Gaussian order of the EDF dependence on laser intensity compared to simulations. (Online version in colour.)

at LLE includes advanced diagnostics, theory, modelling and simulation, experimental platforms and the development of new laser technologies. Several of the highlights of the ongoing research are summarized in this publication and additional detail can be found in the included references.

Since the demonstration of the laser, optical Thomson scattering has been a major diagnostic to measure the macroscopic properties (density, temperature, velocity) of plasmas [37]. In the analysis of the Thomson-scattered light, it is generally assumed that the electron distribution function (EDF) is Maxwellian. However, in laser plasmas, deviations from a Maxwellian electron energy distribution function can arise in both the low-energy bulk electrons since the inverse bremsstrahlung heating rate scales as $(v_e)^{-3}$ and in the high-energy tail where electrons can be heated by processes such as the two-plasmon decay and SRS [16]. The details of the distribution function are critical since it impacts radiation physics (opacity and the use of spectroscopic signatures to characterize plasma conditions), thermal transport and laser–plasma coupling.

With this motivation, LLE has developed an advanced optical Thomson scattering system that enables measurement of the EDF over four orders of magnitude [38]. The diagnostic employs an innovative optical collection system that comprises a primary and secondary aspheric mirror that enables scattered light to be collected over 120° with 1° of resolution. Since the k spectrum of the plasma fluctuations is determined by the wavenumbers of the probe and scattered light

$$k^2 = k_0^2 + k_s^2 - 2k_0 k_s \cos\theta, \tag{5.1}$$

(k_0, k_s are the Thomson probe and the scattered-light wavenumber and θ the angle between them) by measuring over such a wide range of angles, both collective ($k\lambda_D > 1$) and non-collective ($k\lambda_D < 1$) scattering can be measured (λ_D is the plasma Debye length) [37]. This diagnostic allows the EDF to be measured over a large dynamic range in a single experiment.

Figure 14 shows (*a*) a schematic of the diagnostic, (*b*) how the different scattering angles probe different parts of the EDF, and (*c*) the experimental deviations derived from the Thomson-scattered data and characterized by the super-Gaussian order of the distribution
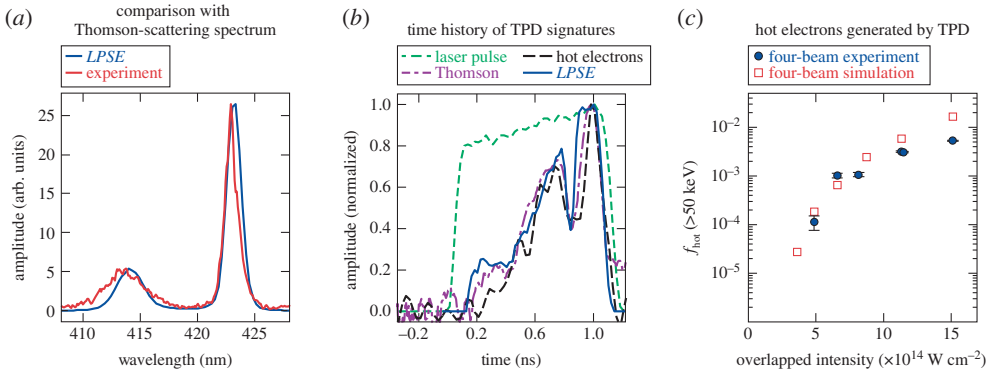
Figure 15. (*a*) OTS scattered-light spectrum compared to *LPSE* simulated output. (*b*) Time history of OTS scattered light compared to *LPSE* simulation. (*c*) Two-plasmon-decay-generated hot electrons inferred from X-ray measurements compared to *LPSE* simulations. (Online version in colour.)

function as a function of laser intensity compared to theory developed by Langdon & Matte [39–41].

Modelling and simulation are also essential components of LPI research. LLE employs a number of simulation codes including *LPSE*, the newly developed Vlasov–Maxwell code *ARGOS*, *LSP*, *VPIC* and *OSIRIS* to design and interpret experiments, to develop reduced models that can be incorporated in Rad-Hydro codes, and to scale the results and define the requirements for MJ-scale drivers for ignition [42–44]. *LPSE* (L̲aser P̲lasma S̲imulation E̲nvironment) is a computational framework for studying laser–plasma interactions relevant to ICF from the microscopic scale of a single laser wavelength to the macroscopic scale of multiple-interacting laser beams [45]. *LPSE* features 3-D non-paraxial wave propagation, injection of arbitrary and realistic laser pulses with speckle, polarization and bandwidth, and shared and distributed memory parallelization, and includes physics models for a number of LPI processes, such as CBET, $2\omega_{pe}$, SRS, resonance absorption, hot-electron generation and nonlinear saturation through the formation of weak turbulence. A powerful capability of *LPSE* is that these processes can be simulated simultaneously or turned on or off to understand how they affect one another. In addition, *LPSE* has post-processing subroutines to generate observables that are measured in experiments. Figure 15 shows comparisons of *LPSE* output with an OTS scattered-light spectrum from $2\omega_{pe}$-driven plasma waves, the time history of the scattered OTS light from $2\omega_{pe}$ and the hot-electron levels inferred from hard X-ray measurements with a characteristic temperature of approximately 40–50 keV.

In addition to innovative diagnostics and modelling/simulation tools, a novel platform for LPI research has been established that combines both the 60-beam OMEGA and an OMEGA EP beam and a flexible plasma source [46]. Laser–plasma research is extremely challenging because of the interdependence of the plasma hydrodynamics and the laser-driven instabilities. In order to isolate the LPI physics from the hydrodynamics, a gas-jet platform was developed on OMEGA that has the required access for OTS to characterize the plasma. This platform provides ideal plasma conditions for studying ignition-relevant LPI. The platform is capable of employing a wide range of gases and the beams of OMEGA 60 are used to create mm-scale plasmas over a range of Z, electron densities and temperature up to near 10^{21} cm^{-3} and 2 keV, respectively. Electron densities up to $n_c/4$ for 35-nm radiation are planned for the future. In addition to the plasma source, a tunable (351 nm ± 1.5 nm) independent beam from OMEGA EP has been transported to the OMEGA-60 target chamber [46]. Initial experiments have used this tunable OMEGA Port 9 (TOP9) beam to study CBET in a stationary plasma [47]. This novel experimental platform is shown in figure 16. By crossing OMEGA (351-nm) beams with the TOP9 beam, the ion-acoustic resonance can be probed in detail. For intensities and plasma conditions relevant
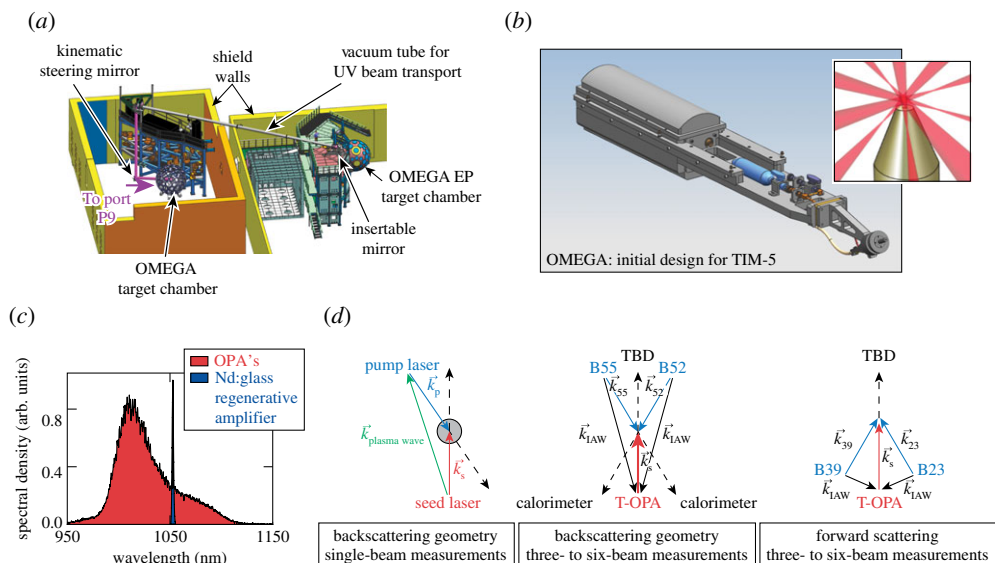
Figure 16. (*a*) TOP9 beam arrangement connecting tunable laser from OMEAG EP to OMEGA 60. (*b*) Target chamber insertable gas-jet target to create a well-diagnosed plasma. (*c*) Tunable laser source spectrum (fundamental Nd:glass wavelength is shown); (*d*) *k* spectrum options for studying CBET in multiple beam and forward and backward configurations. (Online version in colour.)
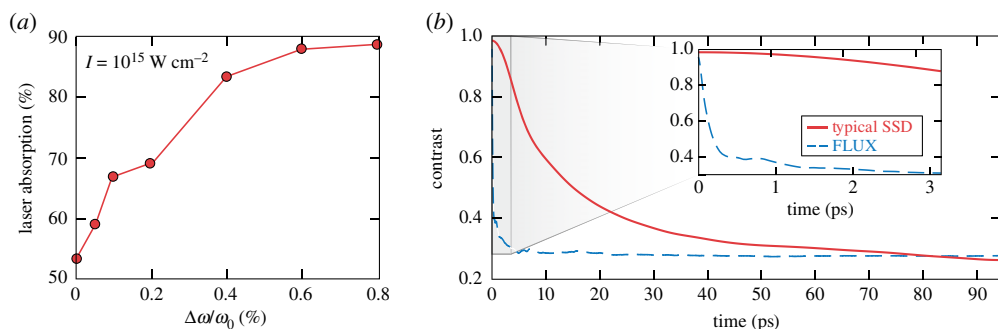

Figure 17. (*a*) *LPSE* calculated target absorption as a function of laser bandwidth; (*b*) single-beam smoothing time for 1% bandwidth laser (FLUX) and the present SSD system on OMEGA 60. (Online version in colour.)

to current ignition studies, these experiments demonstrated the importance of non-Maxwellian electron distribution functions on predicting CBET for example, in the laser-entrance hole of an ICF hohlraum. Future experiments will explore the high-frequency instabilities that produce energetic electrons, including an advanced high-bandwidth laser discussed below.

A critical component of the LPI strategy is to quantitatively understand the physics so as to provide confidence in scaling to ignition-relevant plasmas, and to explore laser-mitigation approaches that will increase the laser–target parameter space for ignition. Theory and modelling have long suggested that reduced laser temporal coherence (proportional to Δv^{-1}, where Δv is the laser bandwidth) can impact LPI if the coherence was comparable to the growth time of the instability [48]. Given nominal experimental parameters bandwidths of the order of 10 THz are required. Figure 17*a* shows *LPSE* results for suppressing CBET and increasing target absorption [49] as a function of fractional bandwidth. Figure 17*b* also shows the significant improvement in laser smoothing that would also drastically reduce laser imprint. With this large bandwidth,
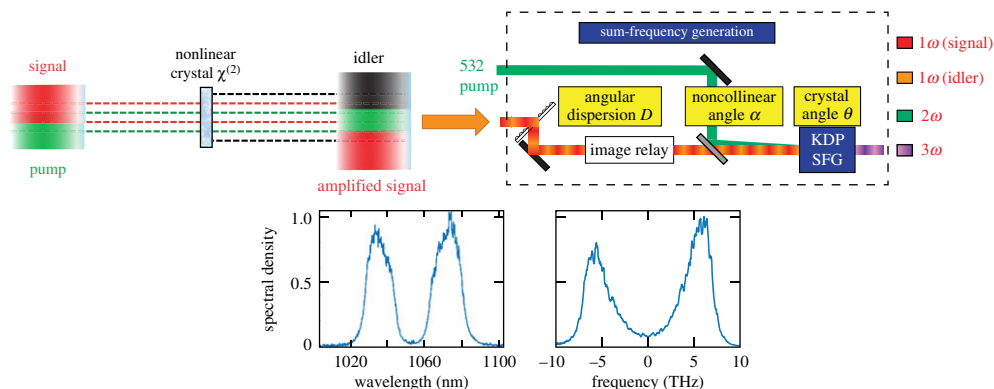
Figure 18. Schematic of advanced laser approach (sum-frequency generation) exploiting optical parametric amplifier technology to generate broadband (greater than 1% bandwidth) UV light (the FLUX laser). (Online version in colour.)

smoothing times are reduced to approximately 1 ps compared to the approximately 100 ps on OMEGA today.

However, present Nd:glass lasers with relatively long upper-state storage times (hundreds of microseconds) gain narrowing that occurs with efficient energy extraction, and up-conversion to the third-harmonic limit the laser bandwidth to less than 1 THz [13]. Optical parametric amplification (OPA) developed for ultrashort pulse offers a potential method to achieve the large bandwidths required for ICF [50]. An OPA laser employs a deuterated KDP crystal pumped by narrowband 526.5-nm light to amplify a broad bandwidth 1053-nm input. The output includes both amplified broadband signal and idler beams. To convert this broadband infrared light into broadband UV radiation, scientists at LLE have developed a novel configuration for sum-frequency generation shown schematically in figure 18 that mixes narrowband 526.5-nm light with broadband 1053 nm light and uses both the amplified signal and idler to achieve bandwidths greater than 10 THz in the UV [51]. Low-energy experiments have validated this technique and the development of a 100-J class laser, the Fourth-generation Laser for Ultrabroadband eXperiments (FLUX), is underway. When complete, over the next several years this beam will be transported to the OMEGA-60 chamber for experiments similar to the strategy employed for the TOP9 beam. Experiments will explore the effect of bandwidth in different spectral formats on both LPI and laser imprint [21].

6. Summary

LDD continues to make progress toward the goal of achieving fusion ignition and gain in the laboratory. The advantages of coupling more laser energy to the capsule reducing the requirements for central hot-spot pressure, convergence and adiabat have become more apparent over the past decade of research on the NIF. Research to quantitatively understand and to identify mitigation degradation mechanisms that reduce the performance of implosions on OMEGA will continue to be a goal emphasizing systematic experiments and 3-D diagnostics and simulations. Conducting LDD research on both the NIF and OMEGA that address LPI physics and hydro scaling will remain a central strategy to provide confidence in projecting LDD understanding to MJ drivers such as the NIF. Limited LDD implosions with a goal of producing approximately 100 kJ of fusion yield will also continue since they are valuable platforms to validate and improve modelling and simulation tools over the range of laser energy and power available on OMEGA and the NIF. Fundamental research on LPI physics will also continue to be a major LDD focus. A quantitative understanding is required to scale the physics to MJ lasers. This research also must include advances in laser technology motivated by the physics that have been learned over

the past decade. Fusion in the laboratory remains a grand scientific challenge and while much progress has been made, challenges remain. Exploiting the increased understanding, modelling tools, diagnostics and advanced laser technologies that have been developed, the next decade presents a great opportunity to make significant progress to this goal.

References

1. Nuckolls J, Wood L, Thiessen A, Zimmerman G. 1972 Laser compression of matter to super-high densities: thermonuclear (CTR) applications. *Nature* **239**, 139–142. (doi:10.1038/239139a0)
2. Lindl JD. 1998 *Inertial confinement fusion: the quest for ignition and energy gain using indirect drive*. New York, NY: Springer.
3. Betti R, Hurricane OA. 2016 Inertial-confinement fusion with lasers. *Nat. Phys.* **12**, 435–448. (doi:10.1038/nphys3736)
4. Sinars DB *et al.* 2020 Review of pulsed power-driven high energy density physics research on Z at Sandia. *Phys. Plasmas* **27**, 070501. (doi:10.1063/5.0007476)
5. Campbell EM, Hogan WJ. 1999 The National Ignition Facility—Applications for inertial fusion energy and high-energy-density science. *Plasma Phys. Control. Fusion* **41**, B39–B56. (doi:10.1088/0741-3335/41/12B/303)
6. Miller GH, Moses EI, Wuest CR. 2004 The National Ignition Facility. *Opt. Eng.* **43**, 2841–2853. (doi:10.1117/1.1814767)
7. Campbell EM *et al.* 2017 Laser-direct-drive program: promise, challenge, and path forward. *Matter Radiat. Extremes* **2**, 37–54. (doi:10.1016/j.mre.2017.03.001)
8. Goncharov VN *et al.* 2017 National Direct-Drive Program on OMEGA and the National Ignition Facility. *Plasma Phys. Control. Fusion* **59**, 014008. (doi:10.1088/0741-3335/59/1/014008)
9. Betti R, Christopherson AR, Spears BK, Nora R, Bose A, Howard J, Woo KM, Edwards MJ, Sanz J. 2015 Alpha heating and burning plasmas in inertial confinement fusion. *Phys. Rev. Lett.* **114**, 255003. (doi:10.1103/PhysRevLett.114.255003)
10. Christopherson AR, Betti R, Lindl JD. 2019 Thermonuclear ignition and the onset of propagating burn in inertial fusion implosions. *Phys. Rev. E* **99**, 021201(R). (doi:10.1103/PhysRevE.99.021201)
11. Collins TJB *et al.* 2012 A polar-drive–ignition design for the National Ignition Facility. *Phys. Plasmas* **19**, 056308. (doi:10.1063/1.3693969)
12. Kessler TJ, Lin Y, Armstrong JJ, Velazquez B. 1993 Phase conversion of lasers with low-loss distributed phase plates. *Proc. SPIE* **1870**, 95–104. (doi:10.1117/12.154474)
13. Skupsky S, Short RW, Kessler T, Craxton RS, Letzring S, Soures JW. 1989 Improved laser-beam uniformity using the angular dispersion of frequency-modulated light. *J. Appl. Phys.* **66**, 3456–3462. (doi:10.1063/1.344101)

14. Lehmberg RH, Obenschain SP. 1983 Use of induced spatial incoherence for uniform illumination of laser fusion targets. *Opt. Commun.* **46**, 27–31. (doi:10.1016/0030-4018(83)90024-X)
15. Soures JM *et al.* 1996 Direct-drive laser-fusion experiments with the OMEGA, 60-beam, >40-kJ, ultraviolet laser system. *Phys. Plasmas* **3**, 2108–2112. (doi:10.1063/1.871662)
16. Kruer WL. 2003 *The physics of laser plasma interactions*, 1st edn. Boca Raton, FL: CRC Press.
17. Randall CJ, Albritton JR, Thomson JJ. 1981 Theory and simulation of stimulated Brillouin scatter excited by nonabsorbed light in laser fusion systems. *Phys. Fluids* **24**, 1474–1484. (doi:10.1063/1.863551)
18. Marozas JA *et al.* 2018 Wavelength-detuning cross-beam energy transfer mitigation scheme for direct drive: Modeling and evidence from National Ignition Facility implosions. *Phys. Plasmas* **25**, 056314. (doi:10.1063/1.5022181)
19. Mannion OM *et al.* 2020 Mitigation of mode-one asymmetry in laser direct-drive inertial confinement fusion implosions. *Phys. Plasmas*.
20. Rinderknecht HG, Casey DT, Hatarik R, Bionta RM, MacGowan BJ, Patel P, Landen OL, Hartouni EP, Hurricane OA. 2020 Azimuthal drive asymmetry in inertial confinement fusion implosions on the National Ignition Facility. *Phys. Rev. Lett.* **124**, 145002. (doi:10.1103/PhysRevLett.124.145002)
21. 28 May 2020 Laser-direct-drive ignition approach report. 2020 *NNSA 2020 Red team review*. Rochester, NY: Laboratory for Laser Energetics, University of Rochester.
22. Gopalaswamy V *et al.* 2019 Tripled yield in direct-drive laser fusion through statistical modelling. *Nature* **565**, 581–586. (doi:10.1038/s41586-019-0877-0)
23. Nora R *et al.* 2014 Theory of hydro-equivalent ignition for inertial fusion and its applications to OMEGA and the National Ignition Facility. *Phys. Plasmas* **21**, 056316. (doi:10.1063/1.4875331)
24. Campbell EM, Hunt JT, Bliss ES, Speck DR, Drake RP. 1986 Nova experimental facility (invited). *Rev. Sci. Instrum.* **57**, 2101–2106. (doi:10.1063/1.1138755)
25. Rosenberg MJ *et al.* 2018 Origins and scaling of hot-electron preheat in ignition-scale direct-drive inertial confinement fusion experiments. *Phys. Rev. Lett.* **120**, 055001. (doi:10.1103/PhysRevLett.120.055001)
26. Spaeth ML *et al.* 2016 Description of the NIF laser. *Fusion Sci. Technol.* **69**, 25–145. (doi:10.13182/FST15-144)
27. Collins TJB, Marozas JA. 2018 Mitigation of cross-beam energy transfer in ignition-scale polar-direct-drive target designs for the National Ignition Facility. *Phys. Plasmas* **25**, 072706. (doi:10.1063/1.5039513)
28. Solodov AA *et al.* 2020 Hot-electron generation at direct-drive ignition-relevant plasma conditions at the National Ignition Facility. *Phys. Plasmas* **27**, 052706. (doi:10.1063/1.5134044)
29. Drake RP, Turner RE, Lasinski BF, Estabrook KG, Campbell EM, Wang CL, Phillion DW, Williams EA, Kruer WL. 1984 Efficient Raman sidescatter and hot-electron production in laser-plasma interaction experiments. *Phys. Rev. Lett.* **53**, 1739–1742. (doi:10.1103/PhysRevLett.53.1739)
30. Seka W, Edgell DH, Myatt JF, Maximov AV, Short RW, Goncharov VN, Baldis HA. 2009 Two-plasmon-decay instability in direct-drive inertial confinement fusion experiments. *Phys. Plasmas* **16**, 052701. (doi:10.1063/1.3125242)
31. Yaakobi B, Solodov AA, Myatt JF, Delettrez JA, Stoeckl C, Froula DH. 2013 Measurements of the divergence of fast electrons in laser-irradiated spherical targets. *Phys. Plasmas* **20**, 092706. (doi:10.1063/1.4824008)
32. Christopherson AR *et al.* 2020 Direct measurements of DT fuel preheat from hot electrons in direct-drive inertial confinement fusion. *Phys. Rev. Lett.*
33. Marozas J *et al.* 2020 High yield, high adiabat polar direct drive target experiments on the National Ignition Facility. *Phys. Plasmas*.
34. Zheng W *et al.* 2016 Laser performance of the SG-III laser facility. *High Power Laser Sci. Eng.* **4**, e21. (doi:10.1017/hpl.2016.20)
35. Miquel JL, Lion C, Vivini P. 2016 The Laser Mega-Joule: LMJ & PETAL status and program overview. *J. Phys.: Conf. Ser.* **688**, 012067. (doi:10.1088/1742-6596/688/1/012067)
36. Obenschain S, Lehmberg R, Kehne D, Hegeler F, Wolford M, Sethian J, Weaver J, Karasik M. 2015 High-energy krypton fluoride lasers for inertial fusion. *Appl. Opt.* **54**, F103–F122. (doi:10.1364/AO.54.00F103)

37. Froula DH, Glenzer SH, Luhmann Jr NC, Sheffield J. 2011 *Plasma scattering of electromagnetic radiation: theory and measurement techniques*, 2nd edn. Amsterdam, The Netherlands: Academic Press.

38. Milder AL *et al.* 2020 Evolution of the electron distribution function in the presence of inverse bremsstrahlung heating and collisional ionization. *Phys. Rev. Lett.* **124**, 025001. (doi:10.1103/PhysRevLett.124.025001)

39. Langdon AB. 1980 Nonlinear inverse bremsstrahlung and heated-electron distributions. *Phys. Rev. Lett.* **44**, 575–579. (doi:10.1103/PhysRevLett.44.575)

40. Matte JP, Lamoureux M, Möller C, Yin RY, Delettrez J, Virmont J, Johnston TW. 1988 Non-Maxwellian electron distributions and continuum X-ray emission in inverse bremsstrahlung heated plasmas. *Plasma Phys. Control. Fusion* **30**, 1665–1689. (doi:10.1088/0741-3335/30/12/004)

41. Afeyan BB, Chou AE, Matte JP, Town RPJ, Kruer WL. 1998 Kinetic theory of electron-plasma and ion-acoustic waves in nonuniformly heated laser plasmas. *Phys. Rev. Lett.* **80**, 2322–2325. (doi:10.1103/PhysRevLett.80.2322)

42. Follett RK, Shaw JG, Myatt JF, Dorrer C, Froula DH, Palastro JP. 2019 Thresholds of absolute instabilities driven by a broadband laser. *Phys. Plasmas* **26**, 062111. (doi:10.1063/1.5098479)

43. Bowers KJ, Albright BJ, Yin L, Bergen B, Kwan TJT. 2008 Ultrahigh performance three-dimensional electromagnetic relativistic kinetic plasma simulation. *Phys. Plasmas* **15**, 055703. (doi:10.1063/1.2840133)

44. Fonseca RA *et al.* 2002 OSIRIS: A three-dimensional, fully relativistic particle in cell code for modeling plasma based accelerators. In *Computational science – ICCS 2002* , vol. 2331 (eds PMA Sloot, CJK Tan, JJ Dongarra, AG Goekstra), pp. 342–351. Lecture notes in computer science. Berlin, Germany: Springer.

45. Myatt JF, Shaw JG, Follett RK, Edgell DH, Froula DH, Palastro JP, Goncharov VN. 2019 *LPSE*: A 3-D wave-based model of cross-beam energy transfer in laser-irradiated plasmas. *J. Comput. Phys.* **399**, 108916. (doi:10.1016/j.jcp.2019.108916)

46. Kruschwitz BE *et al.* 2019 Tunable UV upgrade on OMEGA EP. *Proc. SPIE* **10898**, 1089804. (doi:10.1117/12.2505419)

47. Turnbull D *et al.* 2020 Impact of the Langdon effect on crossed-beam energy transfer. *Nat. Phys.* **16**, 181–185. (doi:10.1038/s41567-019-0725-z)

48. Eimerl D, Kruer WL, Campbell EM. 1992 Ultrabroad bandwidth for suppression of laser driven parametric instabilities. *Comments Plasma Phys. Control. Fusion* **15**, 85–104.

49. Bates JW, Myatt JF, Shaw JG, Follett RK, Weaver JL, Lehmberg RH, Obenschain SP. 2018 Mitigation of cross-beam energy transfer in inertial-confinement-fusion plasmas with enhanced laser bandwidth. *Phys. Rev. E* **97**, 061202(R). (doi:10.1103/PhysRevE.97.061202)

50. Magnitskii SA, Malachova VI, Tarasevich AP, Tunkin VG, Yakubovich SD. 1986 Generation of bandwidth-limited tunable picosecond pulses by injection-locked optical parametric oscillators. *Opt. Lett.* **11**, 18–20. (doi:10.1364/OL.11.000018)

51. Dorrer C, Hill EM, Zuegel JD. 2020 High-energy parametric amplification of spectrally incoherent broadband pulses. *Opt. Express* **28**, 451–471. (doi:10.1364/OE.28.000451)